Vol. 43, No. 2 (2021) 274-282, DOI: 10.24874/ti.1013.11.20.01

Tribology in Industry

www.tribology.rs

RESEARCH

Experimental Investigation of the Effects of Process Parameters on Cutting Force in External Cylindrical Grinding

T.-L. Nguyen[a], V.T. Thai[a,*], L. Hoang[b]

[a]*Faculty of Mechanical Engineering, Hanoi University of Industry, Hanoi, 100000, Vietnam,*
[b]*School of Mechanical Engineering, Hanoi University of Science and Technology, Hanoi, 100000, Vietnam.*

Keywords:

Surface roughness
Cutting force
Cylindrical grinding
Mathematical model
Alloy steel

* Corresponding author:

VanTrong Thai
E-mail: trongtv@haui.edu.vn

Received: 27 November 2020
Revised: 23 December 2020
Accepted: 23 January 2021

A B S T R A C T

Cutting force is a vital parameter that affects product quality. Proper control of the cutting force helps optimize the production process as it improves productivity and product quality. This paper assesses the influence of machining parameters, such as alloy steel hardness and workpiece diameters, to cutting forces when external cylindrical grinding by experimental methods. The cutting force was measured using a workpiece shaft-mounted sensor with a balanced bridge-type resistor sensor. Steel for testing: 40Cr, 9CrSi, 65Mn, and W18Cr4V, which were heat-treated at three different hardness levels: 40, 50, and 60 HRC. The Taguchi method's experimental results show that the main parameters affecting cutting forces are: Feed rate of the grinding wheel S_d, cutting depth t, and hardness of workpiece material on the HRC scale. Since then, we built a mathematical model of the normal cutting force function F_n and tangent cutting force function F_t according to S_d, t, and HRC of 9CrSi steel then tested again with three steel types: 40Cr, 65Mn, and W18Cr4V for quite similar results. The cutting force is controlled through cutting parameters suitable for different hardness and workpiece material based on this model.

1. INTRODUCTION

External cylindrical grinding is one of the methods of finishing the shaft details. The cutting force that occurs when grinding causes vibration, changes the temperature on the workpiece and the cutting tool, affects surface roughness and size error of the product. The cutting force in the external cylindrical grinding process is divided into three components [1-3], shown in Figure 1.

- The force coinciding with the tool direction is called axial force, denoted by F_a. The axial force is relatively small compared to the other two components, so the calculation is often ignored.
- The force preventing the penetration of abrasive particles from getting into the workpiece and is perpendicular to the grinding wheel's cutting surface is called the normal force or the radial force, denoted by F_n.

- The force exerted on the grinding wheel in the direction of the main movement, tangent to the grinding wheel surface, is called tangential force, denoted by F_t.

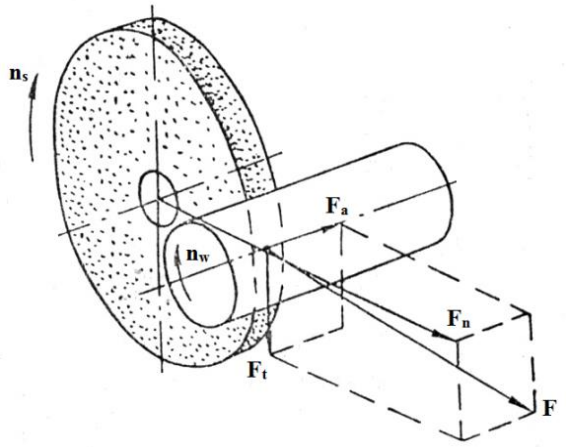

Fig. 1. Cutting force components when external grinding.

Cutting force is an intermediate parameter of the machining process, it depends on the input parameters and affects the output parameters. Thus, it can be seen that the cutting force directly affects the quality of the product. This study aims to determine the influence of machining parameters and machining materials on the cutting force in the external cylindrical grinding process, thereby improving the product's surface quality and accuracy.

2. LITERATURE REVIEW

In the external cylindrical grinding process, the cutting force is a complex dynamic parameter. It depends on such factors as machining mode, machining material, grinding wheel, the vibration of the technology system, the diameter of the workpiece, etc. Therefore, studying to control the cutting force is of great importance, and there have been some studies on this topic. For example, the study [4] analyzed wheel topography and grit force for grinding process modeling. Hecker [5] introduced predictive modeling of grinding force and power based on the probabilistic distribution of undeformed chip thickness as a function of the kinematic conditions, material properties, wheel microstructure, and dynamic effects. Researchers releasing paper [6] used statistical probability theory to predict the number of grains passing through the grinding zone per unit of time. They concluded that only a tiny fraction of the grains participate in the actual cutting process. Jeffrey Badger [7] developed two computer models that can be used to predict the forces generated in grinding and to calculate theoretical grinding charts. Comparisons were made between the predicted forces from each model and the measured forces from grinding experiments. Pavel. K [8] presented the grinding forces' experimental study as the relationship between workpiece speed, feed rate, and cut depth. Ivan Pavlenko et al. [9] presented a new method for parameter identification of cutting forces in crankshaft grinding using artificial neural networks. Olodimyr Kalchenko [10] studied cutting forces in grinding with crossed axes of tool and workpiece. The grinding temperature is taken into account by Lishchenko N. V et al. [11] and Smirnov VA [12]. In studies [13] and [14], authors have studied the vibration that occurs during the external cylindrical grinding and have optimized the 9CrSi steel grinding process multiple objectives in which the cutting force is considered as a binding condition of the grinding process. However, there has not been any research using tests to evaluate the degree of influence of machining mode parameters, material hardness parameters, and the workpiece's size to the cutting force when alloy steel is externally ground. This paper aims to construct mathematical models to control the cutting force during the external cylindrical grinding process.

3. MODELING AND ANALYSIS

3.1. Modeling

The centered external cylindrical grinding method is used in this study. The resistive sensor attached to the centerpiece sends data to the A/D conversion data processor to display the computer screen data. The measuring system (Figure 2) and the two-component F_n and F_t measuring force model on an external cylindrical grinding machine (Figure 3) are as below.

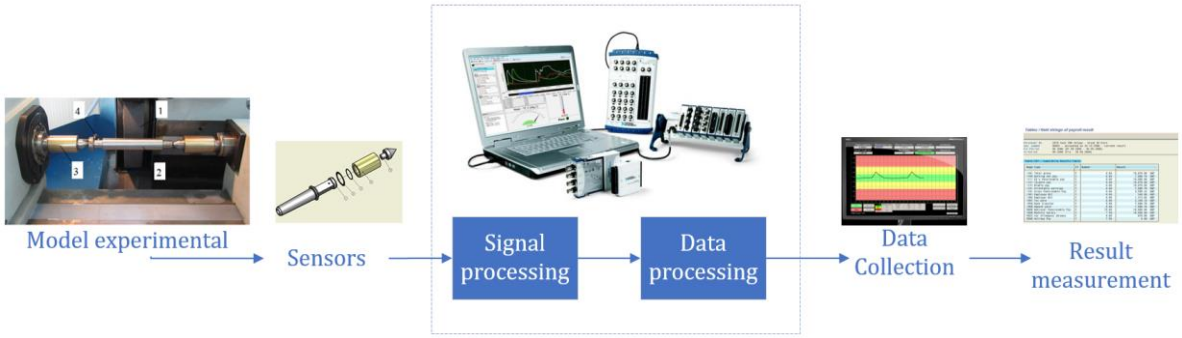

Fig. 2. Block diagram of the measuring system.

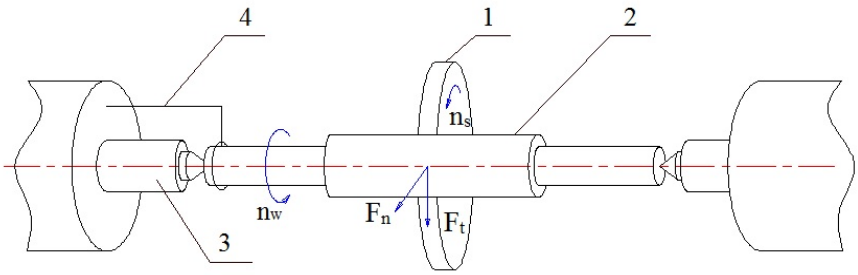

Fig. 3. Force measurement model on external grinding machine, 1- Grinding wheel, 2 – workpiece, 3 – Workpiece shaft-mounted sensor, and 4 – Bar to transmit torque.

3.2. Analysis effect of dimension to cutting force

When the first stage of external cylindrical grinding, named rough grinding, is performed, the workpiece's size affects the cutting force. Figure 4 shows the two workpieces' grinding process with different diameters ($d_1 < d_2$), the same cutting depth t on the same grinding wheel. V_1 and V_2 denote the volume of workpiece 1 and workpiece 2, respectively. Because $V_1 < V_2$, the amount of energy needed to remove V_2 will be more than that to remove V_1. So the cutting force increases when the diameter of the workpiece increases.

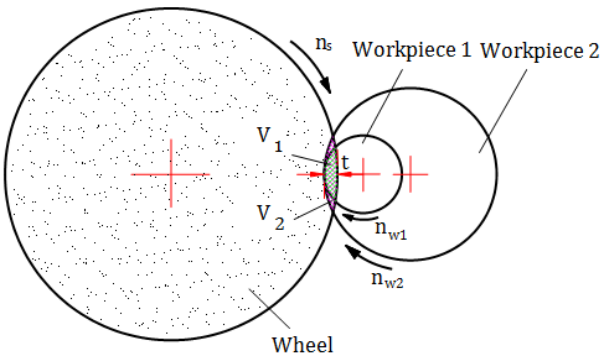

Fig. 4. Model of grinding two workpieces with different diameters with the same cutting depth.

4. MATERIALS AND METHODS

In this study, the experimental design method is used. We use MEG-120 cylindrical grinding machine for the experiments. The grinding wheel rotates at a constant speed of 2000 rpm, the speed of the workpiece is up to 650 rpm, moving speed of the step-less machine table is from 0.1 to 5 m/min. Grinding wheel dimensions are 400x50x203, the grinding grain is Corindon with the particle size from 90 to 63µm, 3-grain diamond stone repairing tool size: 8.5x40, and the cooling method is flood cooling. Workpieces are designed with variable diameters of 20, 30, and 40 mm, the length of grinding long the axis of the workpiece is 70 mm, processing materials are steel 40Cr, 65Mn, 9CrSi, and W18Cr4V treated at high temperature has a hardness value of 40, 50, and 60HRC.

Table 1. Steel brand used for experiments.

Material	Chemical composition (%)	Equivalent
40Cr	C 0.36-0.44, Cr 0.8-1, Mn ≤ 0.8, Si ≤ 0.4, Ni ≤ 0.3	
9CrSi	C 0.85-0.95, Si 1.2-1.6, Mn 0.3-0.6, Cr 0.95-1.25, Mo ≤ 0.2	DIN: 150Cr14
65Mn	C 0.62-0.7, Si 0.17-0.37, Mn 0.9-1.2, Cr ≤ 0.25, Ni ≤ 0.25	
W18Cr4V	C 0.7-0.8, Si ≤ 0,4, Mn ≤ 0.4, Cr 3.8–4.4, V 1-1.4, W 17.5-19	ASTM: T1 tool steel

Workpieces are mounted on the two center points with resistive sensors, the input signal is the real force, and the output signal is a resistor. The impedance difference makes the Wheatstone bridge circuit unbalanced, which creates an mV voltage signal. The small mV signal is amplified thousands of times, which is strong enough to send the corresponding signal to ADC. This signal is encoded and stored in a computer thanks to the ADC. The computer then provides us with reliable technical data that meet manufacturing requirements, as shown in figure 5 and figure 6.

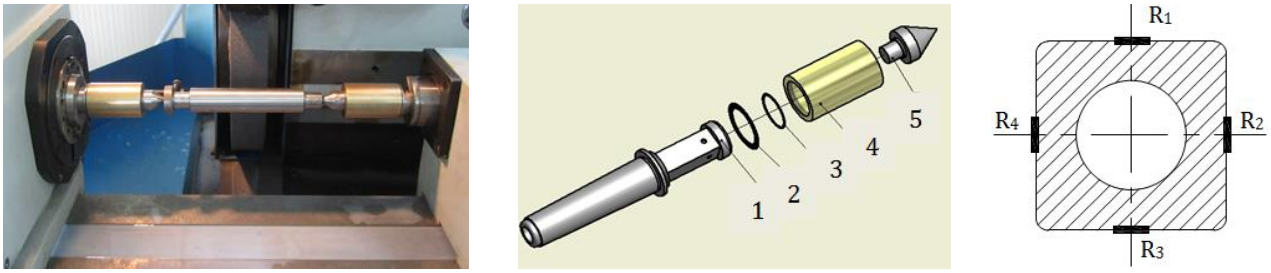

(a) (b) (b)

Fig. 5. Force measurement system on the external circular grinder, (a) Workpiece is mounted on a grinding machine, (b) Center point is mounted with a sensor, with a cover (1 - Sensor body; 2,3 – Grommets; 4 - Sensor ampoule; 5 – Center point), (c) Position stamp on the deformed element.

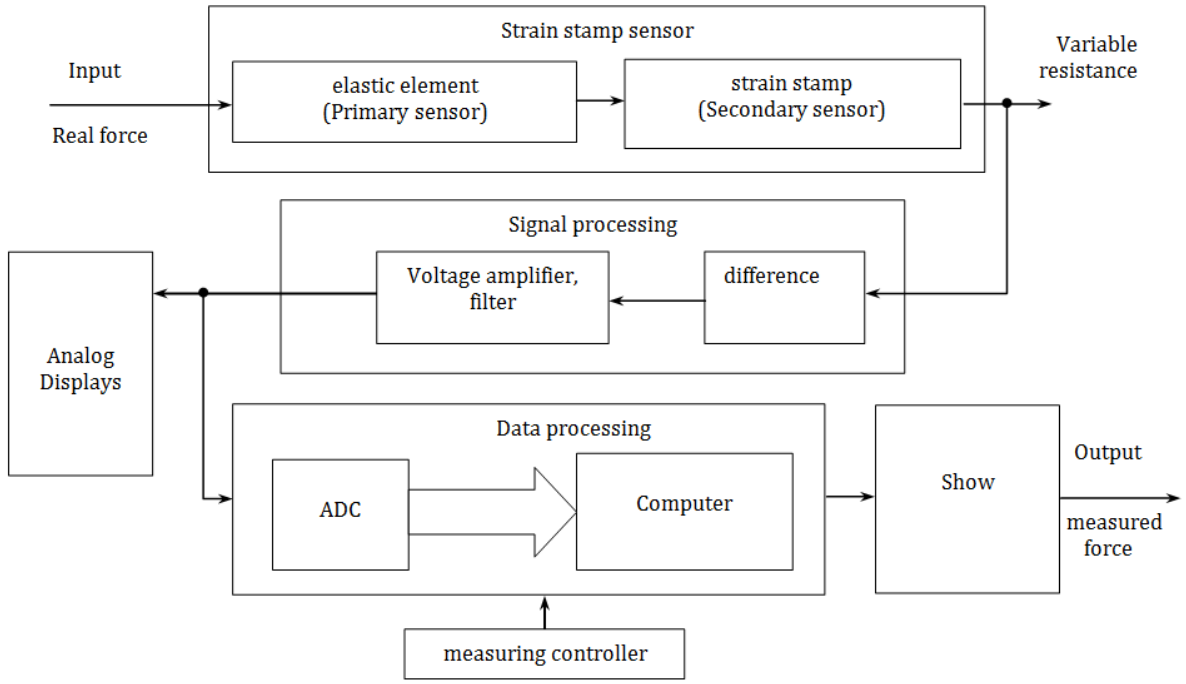

Fig. 6. Block diagram of force measurement with strain stamp sensor.

5. RESULTS AND DISCUSSION

5.1. Measurement results

Studying F_n and F_t when grinding workpieces with hardness are 40 HRC, 50 HRC, and 60 HRC. Changing the workpieces with diameters of 20 mm, 30 mm, and 40 mm respectively, using a fixed machining mode, we have the graphical display of the cutting force on DASYLab10.0 software as shown in figure 7.

Then, we study the cutting force when grinding 9CrSi steel with a hardness value of 50 HRC. Change the grinding wheel's longitudinal feed to three levels: 0.3, 0.4, 0.5 mm/rev. Workpiece speed is set at three levels: 100, 150, 200 rpm. The cutting depth is also set at 3 levels: 0.005, 0.01, 0.02 mm. A graphical display of the cutting force on DASYLab software is shown in Figure 8.

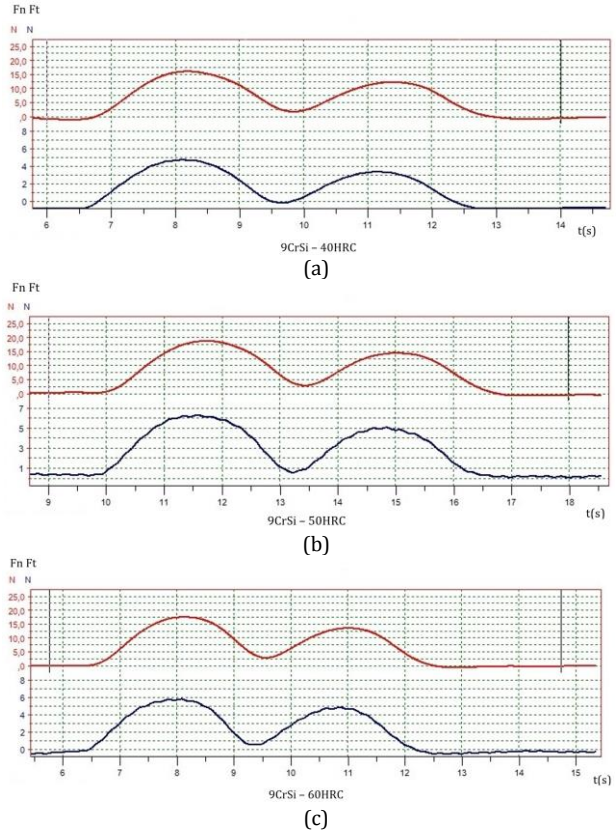

Fig. 7. Cutting force graph when grinding 9CrSi steel (The upper line shows the normal cutting force value F_n, the lower line shows the tangential cutting force F_t value).

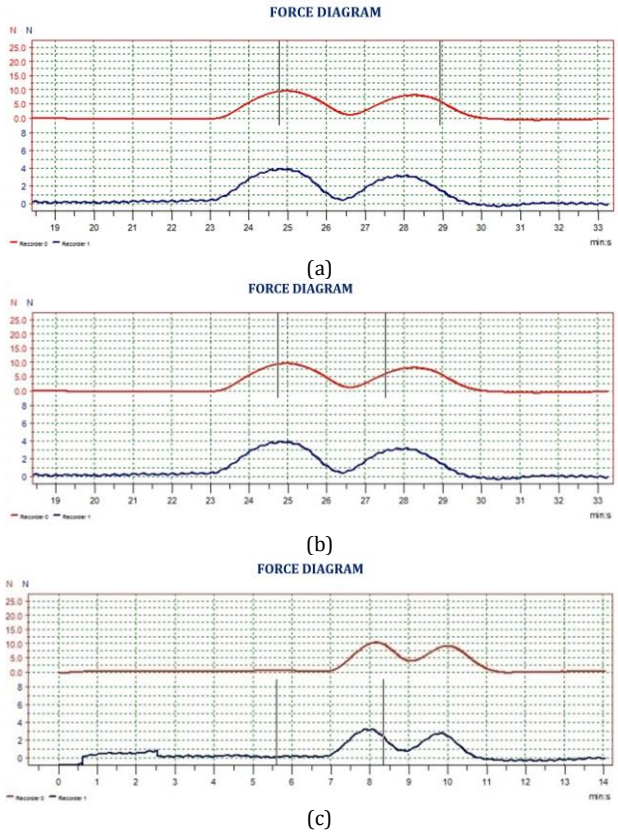

Fig. 8. F_n and F_t cutting force graphs when grinding 9CrSi steel, (a) S_d = 0.4 mm/rev; n_w = 200 rpm; t = 0.005 mm, (b) S_d = 0.4 mm/rev; n_w = 100 rpm; t = 0.01 mm, and (c) S_d = 0.4 mm/rev; n_w = 150 rpm; t = 0.02 mm.

5.2. Analysis of the influence of parameters

Effect of material and workpiece size

An experiment is conducted using 9CrSi alloy with hardness values of 40, 50, 60 HRC. The tested workpiece diameters are 20 mm, 30 mm, 40 mm. The cutting mode is fixed at S_d = 0.5 mm/rev; N_w = 150 rpm; t = 0.01 mm. The two input parameters are different in 3 different experimental conditions. Taguchi L9 orthogonal table is chosen, as shown below [15]:

Table 2. Taguchi L9 orthogonal table with experimental parameters.

No	Hardness HRC	Diameter Dw (mm)	Order of measurement times					
			Fn1 (N)	Fn2 (N)	Fn3 (N)	Ft1 (N)	Ft2 (N)	Ft3 (N)
1	40	20	15.53	15.45	15.46	4.95	4.92	4.96
2	40	30	16.55	16.22	16.34	5.23	5.21	5.25
3	40	40	17.21	17.11	17.15	5.54	5.55	5.55
4	50	20	16.92	16.89	16.90	5.35	5.31	5.34
5	50	30	17.89	17.90	17.88	5.90	5.85	5.86
6	50	40	18.99	19.01	19.12	6.23	6.22	6.31
7	60	20	19.96	19.99	20.05	6.22	6.22	6.25
8	60	30	20.50	20.45	20.55	6.89	6.92	6.91
9	60	40	21.23	21.22	21.31	7.37	7.41	7.40

The wider the R range is, the more effective the variables will have in the processing process. Looking at the above tables, it is clear that workpiece hardness has more impact on the grinding process than workpiece diameter. Thus, we will only control workpiece hardness and ignore workpiece diameter due to its minor influence in grinding. Experiments conducted with 40Cr, 65Mn, and W18Cr4V alloy steels produce the same results. Signal to Noise ratio (SN) analyzed results are as follows:

Table 3. Degree of influence of experimental parameters.

Level	F_n		F_t	
	SN calculated for hardness	SN calculated for diameter	SN calculated for hardness	SN calculated for diameter
1	-24.2551	-24.7918	-14.3771	-14.7701
2	-25.0683	-25.1895	-15.2784	-15.5094
3	-26.2681	-25.6102	-16.684	-16.06
R	**2.013**	**0.8184**	**2.3069**	**1.2899**

Table 4. Taguchi L9 orthogonal table with experimental parameters.

No	S_d (mm/rev)	N_w (rpm)	t (mm)	Order of measurement times					
				F_{n1} (N)	F_{n2} (N)	F_{n3} (N)	F_{t1} (N)	F_{t2} (N)	F_{t3} (N)
1	0.3	100	0.005	6.30	6.14	6.23	1.84	2.02	2.11
2	0.3	150	0.01	6.58	7.02	7.11	2.42	2.68	2.57
3	0.3	200	0.02	11.75	12.11	11.99	4.29	4.54	4.64
4	0.4	100	0.01	10.27	10.01	10.21	3.14	4.01	4.32
5	0.4	150	0.02	16.02	15.89	15.91	5.65	5.46	5.55
6	0.4	200	0.005	9.44	9.45	9.64	3.87	3.99	3.91
7	0.5	100	0.02	22.71	22.25	21.99	7.22	7.10	7.34
8	0.5	150	0.005	13.75	13.79	13.67	4.36	4.45	4.12
9	0.5	200	0.01	15.67	15.55	15.43	5.45	5.23	5.35

Effect of cutting mode parameters

The considered cutting parameters are the longitudinal feed of the grinding wheel S_d, the workpiece rotational speed N_w, and the cutting depth t. The experiment is carried out with 9CrSi alloy with hardness values of 50HRC. Change the grinding wheel's longitudinal feed to three levels: 0.3, 0.4, 0.5mm/rev. Workpiece rotational speed is set at three levels: 100, 150, 200rpm. Cutting depth are also at 3 levels: 0.005, 0.01, 0.02mm. The three input parameters are different in 3 different experimental conditions. Taguchi L9 orthogonal table is chosen as shown in Table 4

Considering R-band shown in Table 5, it can be seen that the longitudinal feed of the grinding wheel Sd and cutting depth t have a great influence on the cutting force, whereas the effect of the workpiece rotational speed on the cutting force is relatively small. Therefore, workpiece rotational speed will be considered an uncontrolled parameter. Experiments conducted with 40Cr, 65Mn, and W18Cr4V alloy steels produce the same results.

Table 5. SN ratio calculated for each indicator and cutting mode.

Level	F_n			F_t		
	SN calculated for S_d	SN calculated for N_w	SN calculated for t	SN calculated for S_d	SN calculated for N_w	SN calculated for t
1	-18.0717	-20.9985	-19.4009	-9.06716	-11.6282	-10.1862
2	-21.2517	-21.1979	-20.254	-12.8294	-11.9157	-11.4803
3	-24.5219	-21.6489	-24.1904	-14.8077	-13.1603	-15.0377
R	**6.4502**	**0.6504**	**4.7895**	**5.7405**	**1.5321**	**4.8515**

5.3. Mathematical model

As shown in section 4.2, the main parameters affecting the cutting force are the longitudinal feed of the grinding wheel S_d, cutting depth t, and HRC hardness of the workpiece. The remaining parameters are uncontrolled parameters and interfering parameters. Thus, we can build the relational function as follows:

$$F = f(S_d, t, HRC) \quad (1)$$

Conducting experiments with 9CrSi steel, we get the following results:

Table 6. Planning table of experimental parameters with steel 9CrSi.

No	Input parameters							F_a (N)	F_t (N)	Ln (S_d)	Ln (t)	Ln (HRC)	Ln (F_n)	Ln (F_t)
	Encoding variable				Experimental variable									
	X_0	X_1	X_2	X_3	S_d (MPM)	t (mm)	HRC							
1	+1	-1	-1	-1	0.3	0.005	40	6.45	2.32	-1.203	-5.298	3.689	1.864	0.842
2	+1	+1	-1	-1	0.5	0.005	40	10.52	3.67	-0.693	-5.298	3.689	2.353	1.300
3	+1	-1	+1	-1	0.3	0.025	40	11.85	4.25	-1.203	-3.912	3.689	2.472	1.447
4	+1	+1	+1	-1	0.5	0.025	40	22.23	7.45	-0.693	-3.912	3.689	3.101	2.008
5	+1	-1	-1	+1	0.3	0.005	60	16.25	5.99	-1.203	-5.298	4.904	2.788	1.790
6	+1	+1	-1	+1	0.5	0.005	60	19.67	7.02	-0.693	-5.298	4.904	2.979	1.949
7	+1	-1	+1	+1	0.3	0.025	60	18.78	6.89	-1.203	-3.912	4.904	2.933	1.930
8	+1	+1	+1	+1	0.5	0.025	60	29.38	12.32	-0.693	-3.912	4.904	3.380	2.511

We build such mathematical models as:

$$F_n = 22.31 S_d^{0.8608} t^{0.3431} HRC^{0.4712} \quad (2)$$

$$F_t = 6.887 S_d^{0.8623} t^{0.3635} HRC^{0.5315} \quad (3)$$

To assess the appropriateness of the regression equation is to check whether the model obtained correctly describes our experiments or not.

We use Fisher standard to compare between Fisher calculation (F_{cal}) and Fisher according to the table (F_{tab}) [16]:

$$F_{cal} < F_{tab}(P, k_1, k_2) \quad (4)$$

In which:

k_1 = N - n – 1 and k_2 = N(m - 1)

N: number of experiments (N = 8)

n: number of factors affecting the test results (n = 3)
m: number of repetitions of the experiment (m = 3)

So: k_1 = 4; k_2 = 16

$$F_{cal} = \frac{S_c^2}{S_r^2} \quad (5)$$

Compatible variance:

$$S_c^2 = \frac{m}{N-n-1}\sum_{i=1}^{N}(\bar{y}_i - \hat{y}_{tb})^2 \quad (6)$$

Repetitive variance:

$$S_r^2 = \frac{1}{N}\sum_{i=1}^{n} S_i^2 = \frac{1}{N(m-1)}\sum_{i=1}^{N}\sum_{j=1}^{m}(y_{ij} - \bar{y}_i)^2 \quad (7)$$

In which:

$\hat{y}_i$: Experimental results No. i calculated according to the regression equation
$\bar{y}_i$: The average value of m times experiments in the i^{th} experiment
y_{ij}: the value of the i^{th} experiment in the j^{th} iteration
$\bar{y}_i - \hat{y}_i$: Error between theory and experiment in an i^{th} experiment.
Basing on experimental results according to Table 5 and the regression "(2)," we have:

$$S_c^2 = 0.0138\,;\ S_r^2 = 0.0119$$

According to the Fisher standard [5]:

$$F_{cal} = 1.16 < F_{tab}(4,16,0.95) = 3.0$$

With "(3),":

$$S_c^2 = 0.0104\,;\ S_r^2 = 0.0089$$

According to the Fisher standard:

$$F_{cal} = 1.17 < F_{tab}(4,16,0.95) = 3.0$$

Thus, mathematical models (2), (3) are consistent with reality.

From "(2)," and "(3),", we built the graphs, as shown in figure 9:

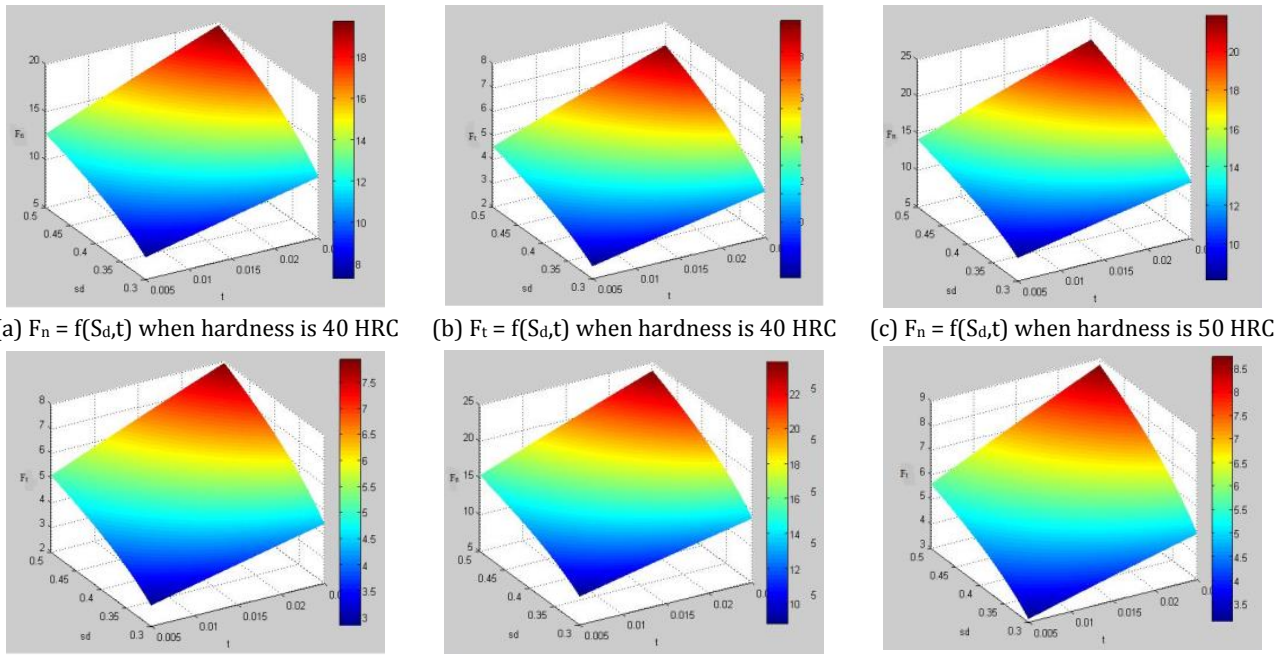

(a) $F_n = f(S_d,t)$ when hardness is 40 HRC (b) $F_t = f(S_d,t)$ when hardness is 40 HRC (c) $F_n = f(S_d,t)$ when hardness is 50 HRC

(d) $F_t = f(S_d,t)$ when hardness is 50 HRC (e) $F_n = f(S_d,t)$ when hardness is 60 HRC (f) $F_t = f(S_d,t)$ when hardness is 60 HRC

Fig. 9. Graphs showing the relationship between cutting force F_n, F_t, and S_d and t when grinding 9CrSi steel.

5.4 Discussion

Conducting experiments with 40Cr steel and experimental processing data (using the same processing methods as in experiments with 9CrSi steel), we get the following results:

$$F_n = 28.663 S_d^{0.8682} t^{0.3556} HRC^{0.3739} \quad (8)$$

$$F_t = 10.837 S_d^{0.8133} t^{0.3585} HRC^{0.3918} \quad (9)$$

With steel 65Mn:

$$F_n = 28.777 S_d^{0.8913} t^{0.3763} HRC^{0.3989} \quad (10)$$

$$F_t = 11.498 S_d^{0.8412} t^{0.3779} HRC^{0.4096} \quad (11)$$

With steel W18Cr4V:

$$F_n = 36.445 S_d^{0.9324} t^{0.3507} HRC^{0.3373} \quad (12)$$

$$F_t = 13.397 S_d^{0.8176} t^{0.3655} HRC^{0.3662} \quad (13)$$

The experimental results show that the normal cutting force F_n is much stronger than the tangential cutting force F_t due to its loss of energy to separate the chip from the material. In grinding, the harder the material is, the more difficult it is for the abrasive grains to enter the material. If the cutting depth is increased, fewer abrasive grains enter the workpiece. As a result, such a phenomenon as sliding on the surface, cutting depth is shallower than required, grinding wheel grows dull, and broken grinding grains appear.

The results in the survey area show that in external cylindrical grinding, the cutting force depends not only on the cutting mode but also on the workpiece's hardness. The cutting force becomes greater when increasing the hardness of the materials, the longitudinal feed of the grinding wheel, and the cutting depth, and the results are tested in experiments with 9CrSi, 40Cr, 65Mn, and W18Cr4V steels.

6. CONCLUSION

1. Successfully measured cutting force with the presented dynamometer.
2. Constructed mathematical models of cutting forces F_n and F_t in the external cylindrical grinding process.
3. Determined that the main parameters affecting cutting forces when the external cylindrical grinding are feed rate, depth of cut, and hardness of the workpiece.
4. When the feed rate increases, the cutting force increases.

5. When the depth of cut increases, the cutting force increases.
6. When the hardness of the workpiece increases, the cutting force increases.
7. When changing to another steel, the rules in conclusion 1, 2, 3 do not change.
8. Determining the external cylindrical cutting force will help control the grinding process to achieve better product quality.
9. Developing this work, we would like to experimental studies that will take into account the effect of the grinding width, and others parameters on the values of the cutting forces. Then, we would like to study the dependence of the roughness on the values of the cutting forces.

REFERENCES

[1] W.B, Rowe, *Principles of Modern Grinding Technology*, William Andrew, 2009, doi: 10.1016/C2013-0-06952-6

[2] F. Klocke, *Manufacturing Processes 2: Grinding, Honing, Lapping*, Springer, 2009, doi: 10.1007/978-3-540-92259-9

[3] C.H. Liu, C-C.A. Chen, C.-Y. Lin, C.-J. Lin, *A Three-Component Strain Gage Dynamometer for Grinding and Polishing Force Measurement*, Journal of Materials Engineering and Performance, vol. 14, no 2, pp. 173-178, 2004, doi: 10.1361/10599490522374

[4] R.L. Hecker, I.M. Ramoneda, S.Y. Liang, *Analysis of wheel topography and grit force for grinding process modeling*, Journal of Manufacturing Processes, vol. 5, iss. 1, pp. 13-23, 2003, doi: 10.1016/S1526-6125(03)70036-X

[5] R.L. Hecker, S.Y. Liang, *Grinding force and power modeling based on chip thickness analysis*, The International Journal of Advanced Manufacturing Technology, vol. 33, iss. 5–6, pp. 449–459, 2007, doi: 10.1007/s00170-006-0473-y

[6] Z.B. Hou, R. Komanduri, *On the mechanics of the grinding process – Part I. Stochastic nature of the grinding process*, International Journal of Machine Tools and Manufacture, vol. 43, iss. 15, 2003, doi: 10.1016/S0890-6955(03)00186-X

[7] J.A. Badger, A.A. Torrance, *Comparison of two models to predict grinding forces from wheel surface topography*, International Journal of Machine Tools and Manufacture, vol. 40, iss. 8, pp. 1099-1120, 2000, doi: 10.1016/S0890-6955(99)00116-9

[8] P. Kovač, M. Gostimirović, *Grinding Force of Cylindrical and Creep-Feed Grinding Modeling*, in Abrasive Technology - Characteristics and Applications, IntechOpen, 2018, doi: 10.5772/intechopen.76968

[9] I. Pavlenko, M. Saga, I. Kuric, A. Kotliar, Y. Basova, J. Trojanowska, V. Ivanov, *Parameter Identification of Cutting Forces in Crankshaft Grinding Using Artificial Neural Networks*, Materials vol. 13, iss. 23, pp. 53-57, 2020, doi: 10.3390/ma13235357

[10] V. Kalchenko, A. Yeroshenko, S. Boyko, N. Sira, *Determination of cutting forces in grinding with crossed axes of tool and workpiece*, Acta Mechanica et Automatica, vol. 11, no. 1, 2017, doi: 10.1515/ama-2017-0009

[11] N.V. Lishchenko, V.P. Larshin, H. Krachunov, *Simplified grinding temperature model study*, Journal of Engineering Sciences, vol. 6, iss. 2, pp. A1-A7, 2019, doi: 10.21272/jes.2019.6(2).a1/

[12] V.A. Smirnov, A.V. Repko, *Workpiece temperature variations during flat peripheral grinding*, Management Systems in Production Engineering, vol. 26, iss. 2, pp. 93-98, 2018, doi: 10.1515/mspe-2018-0015

[13] T.-L. Nguyen, N.-T. Nguyen, L. Hoang, *A study on the vibrations in the external cylindrical grinding process of the alloy steels*, International Journal of Modern Physics B, vol. 34, no. 22n24, pp. 2040150, 2020, doi: 10.1142/S0217979220401505

[14] T.-L. Nguyen, N.-T. Nguyen, L. Hoang, *Multi-objective optimization using the genetic algorithms for the external cylindrical grinding process of 9CrSi alloy*, International Journal of Modern Physics B, vol. 34, iss. 22n24, pp. 2040161, 2020, doi: 10.1142/S021797922040161X

[15] R.K. Roy, *Design of Experiments Using The Taguchi Approach, 16 Steps to Product and Process Improvement*, Wiley, 2001.

[16] D.C. Montgomery, *Design and Analysis of Experiments*, Wiley, 2019.